



Global Love wave overtone measurements

K. Visser,¹ S. Lebedev,¹ J. Trampert,¹ and B. L. N. Kennett²

Received 2 November 2006; revised 20 December 2006; accepted 22 December 2006; published 2 February 2007.

[1] Love wave phase velocities for fundamental and higher modes are difficult to measure because the different modes cannot easily be separated. Following Yoshizawa and Kennett (2002), we generate suites of path specific one-dimensional shear wave velocity profiles using the Neighbourhood Algorithm of Sambridge (1999a). From this family of $O(10^4)$ models both fundamental and higher mode phase velocities with mutually consistent uncertainties are calculated. We have fully automated the method and analysed over forty thousand Love wave seismograms from the GDSN and GEOSCOPE global networks from 1994–2004. Our phase velocity measurements agree remarkably well with previous studies, but we have been able to enlarge the available dataset dramatically. We present global Love wave phase velocity maps (up to the fifth overtone) with unprecedented resolution due to the improved path coverage. Comparing these maps to existing tomographic models, we discern evidence of significant anisotropy in the lower mantle around a depth of 1000 km in the Pacific. **Citation:** Visser, K., S. Lebedev, J. Trampert, and B. L. N. Kennett (2007), Global Love wave overtone measurements, *Geophys. Res. Lett.*, *34*, L03302, doi:10.1029/2006GL028671.

1. Introduction

[2] Phase velocity maps have mainly been constructed for fundamental mode surface waves. The sensitivity of fundamental modes, at commonly used periods up to 200 seconds, is limited to the upper 400 km. Surface wave tomography using such modes, therefore, suffers from a limited depth penetration. The obvious way to increase depth penetration is to add higher mode information. The sensitivities of higher modes extend well below the transition zone and into the lower mantle. Techniques to measure higher mode surface wave phase velocities are mostly based on the separation of modes in the seismogram and can be roughly divided into two groups: methods that use clustering of stations [Nolet, 1975; Cara, 1979] or events [Stutzmann and Montagner, 1993; Beucler et al., 2003], and methods that use single seismograms [Van Heijst and Woodhouse, 1999; Yoshizawa and Kennett, 2002]. The disadvantage of using clusters is that the distribution and number of phase velocity measurements is geographically very limited. Van Heijst and Woodhouse [1999] used a mode branch stripping technique to obtain phase velocity

measurements of the fundamental and higher mode surface waves. This method is effective for seismograms with longer paths where the modes are reasonably well separated, and hence is difficult to apply to Love waves where fundamental and higher modes travel closely together. Yoshizawa and Kennett [2002] used a fully non-linear waveform inversion to obtain regional path specific multimode dispersion measurements. This method samples the model space for a depth dependent shear wave velocity model that fits the observations best. This best fitting shear wave model, not meant to be a direct representation of the Earth model, is interpreted as providing implicit information on the multimode dispersion for the given source-receiver path. In carefully chosen frequency windows, mode coupling for the first few modes can be restricted [Kennett, 1995]. Furthermore, a direct interpretation of the path specific models is only valid for small lateral perturbation along the path, whereas less constrictive conditions apply to the corresponding multimode dispersion curves [Kennett and Yoshizawa, 2002]. Yoshizawa and Kennett [2002] obtained approximate standard deviations by comparing the dispersion curves of the 1000 best shear velocity models. From the best fitting model, phase velocities are calculated without any mode separation, in a fully non-linear framework. We develop a fully automated implementation of this approach and improve the uncertainty analysis by calculating complete probability density functions for all phase velocities. This enables us to make multimode dispersion measurements with mutually consistent error estimates. The method is applied to measure fundamental and higher mode Love wave phase velocities on a global scale.

2. Method

[3] In principle, the model space search to invert the seismogram for a 1D velocity model could include the full non-linearity of the forward problem. In practise, time constraints force us to limit the search around a reference model. The use of Fréchet derivatives introduces a dependence of the final result upon the reference model which we obtain from the Automated Multimode Inversion method (AMI) [Lebedev et al., 2005]. This is a waveform inversion technique that uses multiple time and frequency windows to obtain a shear wave velocity model that explains both the fundamental mode as well as the higher modes in the seismogram. The safeguards build into AMI guarantee that the JWKB approximation is valid for all seismograms which provide measurements. The shear wave velocity model from AMI is used to calculate all eigenfunctions and Fréchet derivatives for the model space search. For the search itself we use the Neighbourhood Algorithm (NA) [Sambridge, 1999a, 1999b]. NA involves two separate steps. The first step is a guided Monte Carlo sampling. A

¹Faculty of Geosciences, Utrecht University, Utrecht, Netherlands.

²Research School of Earth Sciences, Australian National University, Canberra, ACT, Australia.

relative least squares misfit M guides the model space search to areas of better fit where the difference between the data (d) and the synthetic seismograms (s) is considered relative to the maximum amplitude in a specific window ($d_{\max}(\mathbf{W})$):

$$M = \sum_{w=1}^N \sum_{i=1}^L \frac{(d_i - s_i)^2}{(d_{\max}(\mathbf{W}))^2} \quad (1)$$

where N is the number of time-frequency windows and L is the number of time samples in each window. The time-frequency windows are chosen such that the fundamental mode is mainly excited in the lower frequency windows (5–20 mHz) and the higher modes are mainly excited in the higher frequency windows (20–50 mHz) (Figures 1a, 1b, and 1c). The lower time limit in the first two windows corresponds to the group arrival with a velocity of 3.8 km/s, which should capture the complete Love wave fundamental mode as long as the perturbations with respect to PREM are not too large. The lower time limit of the third window corresponds to a group velocity of 4.3 km/s to include the higher modes and exclude the fundamental mode. The higher time limit in all windows depends on the epicentral distance, below 35° the time is set just before the arrival of the S wavetrain. Between 35° and 70° the time is set just after the S and before the SS wavetrain etc. For the determination of the left window boundaries, the S and multiple S arrival times are computed using the AK135 model [Kennett *et al.*, 1995].

[4] The synthetic seismogram $s(\omega)$ in the frequency domain is calculated as a sum of modes m using the JWKB approximation:

$$s(\omega) = \sum_m A_m(\omega) \exp[i\omega\Delta/(C_m^0(\omega) + \delta C_m(\omega))], \quad (2)$$

where $A_m(\omega)$ is the complex amplitude of the modes, Δ is the source-receiver distance, $C_m^0(\omega)$ is the Love wave phase velocity in the reference model and $\delta C_m(\omega)$ is a Love wave phase velocity perturbation

$$\delta C_m(\omega) = \int_0^a \left[\frac{\partial C_m^0(\omega)}{\partial V_s(r)} \delta V_s(r) + \frac{\partial C_m^0(\omega)}{\partial \rho(r)} \delta \rho(r) \right] dr. \quad (3)$$

The Fréchet derivatives $\partial C_m^0(\omega)/\partial V_s(r)$ and $\partial C_m^0(\omega)/\partial \rho(r)$ relate the change in shear wave velocity and density from the reference model to changes in the phase velocity. a is the radius of the Earth. The density perturbations are of secondary importance and are scaled to the shear wave velocity perturbations. The scaling relation ($\xi = \partial \ln \rho / \partial \ln V_s$) is taken from Deschamps *et al.* [2001]. We checked that different scaling relations did not alter our results. The attenuation is that of PREM. The change in shear wave velocity $\delta V_s(r)$ is parameterized through a set of 1-D basis functions $h_i(r)$:

$$\delta V_s(r) = \sum_{i=1}^{12} \gamma_i h_i(r), \quad (4)$$

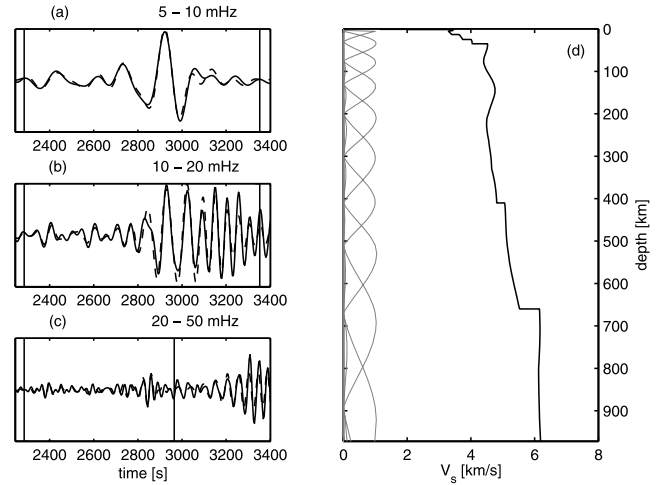


Figure 1. Fit of the data with the synthetics (dashed lines) in three time-frequency windows: (a) 5–10 mHz, (b) 10–20 mHz, (c) 20–50 mHz, and the (d) corresponding shear velocity model for the best fitting model with the spline parameterization. The time-windows are indicated by the vertical bars.

where the γ_i are the coefficients to be found in the model space search. The boundaries of the model space are chosen such that $\pm 2\%$ changes (justification below) are allowed around the reference model.

[5] The functions $h_i(r)$ are twelve natural cubic spline basis functions that span the shear velocity model in the crust, upper mantle and lower mantle up to a depth of 1500 km (Figure 1d). The basis functions are spaced more densely in the crust and upper mantle to match the expected depth resolution of surface waves. We typically sample 5100 models per seismogram ($n_s = 10$, $n_r = 5$, 500 iterations, 100 initial models).

[6] From this first sampling, no stable measurements can be estimated. The second part of the Neighbourhood Algorithm [Sambridge, 1999b] resamples the initial ensemble of models and constructs a conditional posterior probability density function given the seismograms \mathbf{d} .

$$P(\mathbf{m}|\mathbf{d}) = \kappa \rho(\mathbf{m}) L(\mathbf{m}|\mathbf{d}), \quad (5)$$

where $\rho(\mathbf{m})$ is the prior probability distribution (depending on the parameterization, equation (4); search boundaries, $\pm 2\%$; and the forward theory, equations (2) and (3)) and $L(\mathbf{m}|\mathbf{d}) = \exp(-\frac{1}{2}M/c)$ is a likelihood function which represents a fit to the observations. M is defined in equation (1). κ and c are normalization constants.

[7] The statistical properties of the ensemble are defined in a Bayesian framework and are evaluated using Monte Carlo integration [Sambridge, 1999b]. We resample using 1500 models which is sufficient for convergence of the integrals. The results are presented as one-dimensional marginal probabilities for each model parameter by integrating over all other dimensions of the probability density function. The marginal probability densities for the coefficients γ_i (equation (4)) can easily be transformed into marginal probability densities for phase velocities of any mode at any period using equations (3) and (4). Because

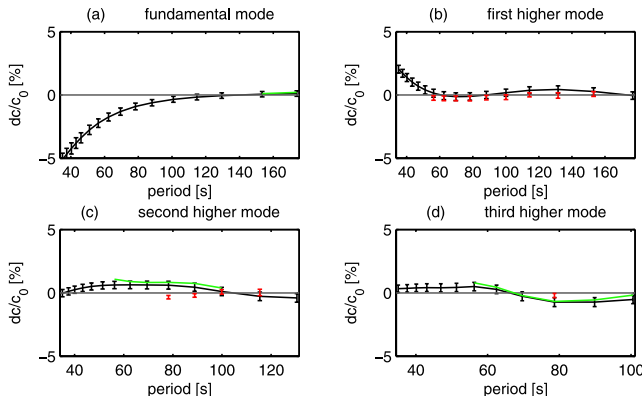


Figure 2. Comparison of phase velocity measurements with respect to PREM for (a) the fundamental mode, (b) the first higher mode, (c) the second higher mode, and (d) the third higher mode. Indicated are measurements of *Van Heijst and Woodhouse* [1999] with standard deviations according to cluster analysis (red) and measurements with AMI as given by *Lebedev et al.* [2006] (green).

of the central limit theorem, we observe that the marginals for phase velocities are close to Gaussian, which can conveniently be described by its mean and standard deviation.

3. How Many Overtones?

[8] In principle, we can calculate the phase velocity of any mode from the 1D Earth model, the important question is thus how many modes are constrained by each seismogram. To obtain a measure of the higher mode information in each seismogram, we investigate the unexplained variance V as a function of the number of modes K in the synthetic seismogram:

$$V(K) = \frac{\sum_{i=1}^L [d_i - s_i(K)]^2}{\sum_{i=1}^L d_i^2}, K = 0, 1, \dots, 30, \quad (6)$$

K is allowed to vary from the fundamental mode only ($K = 0$) to up to 30 higher modes. The unexplained variance is only evaluated in the time-frequency window, which contains the most higher mode information and the least fundamental mode information (Figure 1c), because we want to obtain a measure of the higher mode information available in the seismogram. The unexplained variance with up to K modes $V(K)$ generally decreases with increasing K . The number of overtones constrained by a seismogram is defined as the smallest number of the modes which brings $V(K)$ below 25% of its range, where the range is defined as the difference between the maximum ($V(0)$) and the minimum ($V(30)$) value. This empirical threshold was chosen after visual inspection of the variance curves for numerous seismograms.

[9] In two cases we decide to measure the fundamental mode only: if we obtain a bad fit for the higher modes ($V(30) > 0.5$), or if there is no significant higher mode information in the seismogram ($V(0) < 0.2$). A final test calculates the unexplained variance ($V(30)$) for all three time-frequency windows. If more than 60% of the seismo-

gram ($V(30) > 0.4$) remains unexplained, the seismogram is discarded. From a total of 310,000 seismograms, we measured 14.5% fundamental mode, 11.1% first, 10.1% second, 7.7% third, 4.8% fourth and 2.7% fifth higher mode dispersion curves.

4. Dispersion Measurements

[10] We measured minor arc Love wave phase velocities using data from the GEOSCOPE and GDSN global networks from 1994 to 2004. Figures 1a–1c show an example of the waveform fit obtained in three different time-frequency windows for the best fitting model (Figure 1d) given by the model space search. The corresponding phase velocity measurements are shown in Figure 2 for the fundamental mode and the first, second and third higher modes. The measurements agree well with existing measurements made by *Van Heijst and Woodhouse* [1999] (Figures 2 and 3) and those made with AMI by *Lebedev et al.* [2006] (Figure 2). We calculated uncertainties for Van Heijst’s measurements by cluster analysis.

[11] Our standard deviations do not depend on the quality of the original seismogram because of the definition of the misfit function (equation (1)); they depend mainly on the size of the modelspace. This is again a result of the central limit theorem, which states that the sum of n independent equally distributed random variables will approach a normally distributed random variable as n increases. The resulting standard deviation (but not the mean) is dependent on the standard deviations of the n random variables. The phase velocity marginals are a sum over all shear wave velocity marginals and thus tend towards Gaussian distributions, with a robust mean. The standard deviation of the phase velocity marginal depends on the standard deviations of the shear wave velocity marginals, and hence the a priori size of the modelspace. We can thus not obtain absolute uncertainties from NA, but the relative uncertainties between modes are self consistent. We define the boundaries of the modelspace ($\pm 2\%$ around the AMI reference model) such that the resulting standard deviations for the fundamental mode match the standard deviations obtained by cluster analysis by *Trampert and Woodhouse* [2001]. They

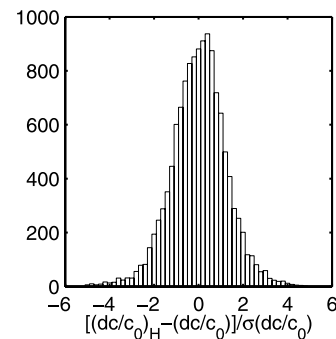


Figure 3. Histogram comparing overtone phase velocity measurements (first, second and third overtone branch) of *Van Heijst and Woodhouse* [1999] ($(dc/c_0)_H$) with this study (dc/c_0) scaled by our standard deviations ($\sigma(dc/c_0)$). 16,756 ($\approx 65\%$) out of a total of 25,908 overlapping measurements fall within one standard deviation.

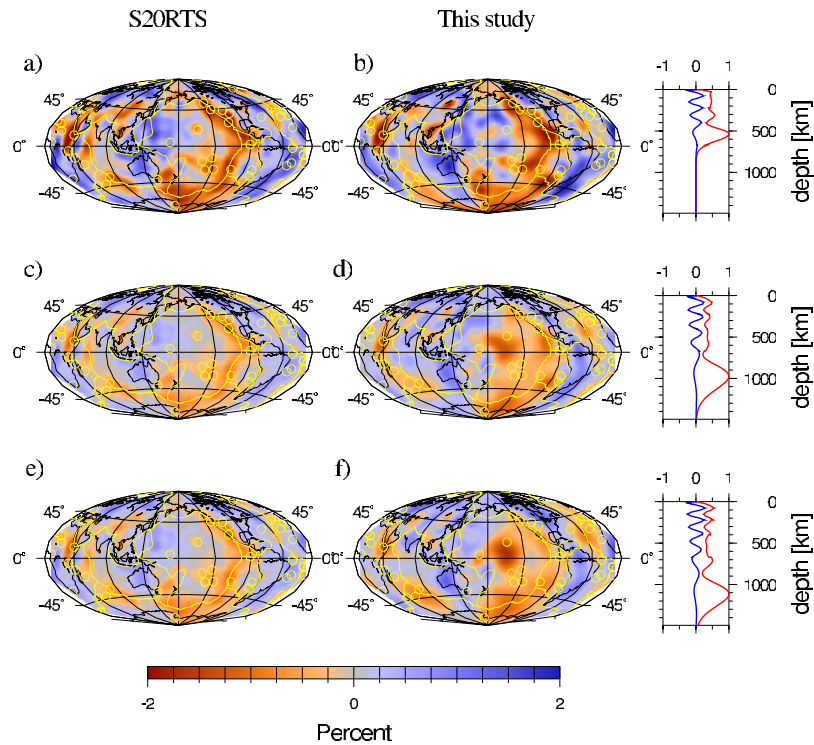


Figure 4. Deviations in Love wave phase velocity dc/c_0 calculated for model S20RTS and the new Love wave measurements. (a, b) Third higher mode at 46.95s; (c, d) fourth higher mode at 62.77s; and (e, f) fifth higher mode at 56.29s. The sensitivity curves (red for V_s and blue for ρ) for the specific modes are displayed to the right.

showed that uncertainties for cluster analysis are in agreement with uncertainties obtained for comparing model predictions to real seismograms. The anchoring will thus turn the self consistent relative uncertainties between modes in realistic absolute uncertainties.

[12] A compact representation of the measurements is to construct phase velocity maps. Figures 4b, 4d, and 4f show global minor arc phase velocity maps for Love waves for the third, fourth and fifth overtone. The phase velocity maps were expanded on a spherical harmonic basis up to degree and order 20, following the same procedure as described by *Trampert and Woodhouse* [1995]. The number of measurements, initial and final χ^2 of the phase velocity maps are given in Table 1. The derivative damping was chosen to allow an easy comparison with predictions for the model S20RTS of *Ritsema et al.* [1999] where the crust was added using CRUST5.1 [Mooney et al., 1998] (Figures 4a, 4c, and 4e). Even for the fifth overtone, the ray density is higher and more uniform than that given by *Trampert and Woodhouse* [1995]. The resolution is then at least as good as that of Figure 7a of *Trampert and Woodhouse* [1995]. Some phase velocity maps (with bulk sensitivities shallower than 1000 km) agree well with the S20RTS prediction (see Figures 4a and 4b), even though the S20RTS model does not contain Love wave information. For higher modes, with main sensitivities around 1000 to 1500 km, there is a discrepancy between the Love wave phase velocity maps and the S20RTS phase velocity maps (Figures 4c–4d and Figures 4e–4f) in the Pacific. The S20RTS model is based on mainly Rayleigh equivalent surface waves. This discrep-

any indicates a difference between SH and SV around 1000 to 1500 km, an indication of anisotropy.

5. Concluding Remarks

[13] We measured higher mode Love wave phase velocities up to the fifth higher mode with corresponding uncertainties using a new, fully automatic procedure. The use of a model space sampling allows us to derive mutually consistent estimates of relative standard deviations between different overtone branches and from measurement to measurement. The phase velocities agree well with existing measurements [Van Heijst and Woodhouse, 1999; Lebedev et al., 2006], especially for the fundamental modes. The higher modes agree well within their standard deviation. The differences between the different techniques are caused by different theoretical formulations; branch stripping (van Heijst) or multiple frequency and time windows (Lebedev). The resulting phase velocity maps agree well with phase velocity maps predicted by the model S20RTS [Ritsema et al., 1999] model. Love wave phase velocity maps with high sensitivities between 1000 and 1500 km differ from the

Table 1. Details for the Phase Velocity Maps of Figure 4

Mode	Period in PREM, s	Number of Measurements	$\chi^2_{initial}$	χ^2_{final}
3	46.95	24,102	4.21	3.28
4	62.77	15,065	2.00	1.75
5	56.29	8,515	2.16	1.96

Rayleigh wave based S20RTS, giving an indication of anisotropy in the Pacific around the Pacific superplume. The use of high quality overtone measurements should improve the resolution in the mid-mantle where the differences between existing models are largest [Romanowicz, 2003].

[14] **Acknowledgments.** We would like to thank M. Sambridge for providing the Neighbourhood Algorithm programs, his suggestions and useful discussions. The data used in this study have been provided by the GDSN and GEOSCOPE networks and obtained via the IRIS database. Figure 4 was generated with the Generic Mapping Tools (GMT) [Wessel and Smith, 1995]. Part of the calculations were performed on a 64 node cluster financed by the Dutch National Science foundation under grant NWO:VICI865.03.007. Other computational resources for this work were provided by the Netherlands Research Center for Integrated Solid Earth Science (ISES 3.2.5 High End Scientific Computation Resources).

References

- Beucler, E., E. Stutzmann, and J. P. Montagner (2003), Surface wave higher mode phase velocity measurements using a roller-coaster type algorithm, *Geophys. J. Int.*, *155*, 289–307.
- Cara, M. (1979), Lateral variations of S velocity in the upper mantle from higher Rayleigh modes, *Geophys. J. R. Astron. Soc.*, *57*, 649–670.
- Deschamps, F., R. Snieder, and J. Trampert (2001), The relative density to shear velocity scaling in the uppermost mantle, *Phys. Earth Planet. Inter.*, *124*, 193–211.
- Kennett, B. L. N. (1995), Approximations for surface-wave propagation in laterally varying media, *Geophys. J. Int.*, *122*, 470–478.
- Kennett, B. L. N., and K. Yoshizawa (2002), A reappraisal of regional surface wave tomography, *Geophys. J. Int.*, *150*, 37–44.
- Kennett, B. L. N., E. R. Engdahl, and R. Buland (1995), Constraints on seismic velocities in the Earth from traveltimes, *Geophys. J. Int.*, *122*, 108–124.
- Lebedev, S., G. Nolet, T. Meier, and R. D. van der Hilst (2005), Automated multimode inversion of surface and S waveforms, *Geophys. J. Int.*, *162*, 951–964.
- Lebedev, S., T. Meier, and R. D. van der Hilst (2006), Asthenospheric flow and origin of volcanism in the Baikal Rift area, *Earth Planet. Sci. Lett.*, *249*, 415–424.
- Mooney, W. D., G. Laske, and T. G. Masters (1998), CRUST 5.1: A global crustal model at $5^\circ \times 5^\circ$, *J. Geophys. Res.*, *103*, 727–748.
- Nolet, G. (1975), Higher Rayleigh modes in western Europe, *Geophys. Res. Lett.*, *2*, 60–62.
- Ritsema, J., H. J. van Heijst, and J. H. Woodhouse (1999), Complex shear wave velocity structure imaged beneath Africa and Iceland, *Science*, *286*, 1925–1928.
- Romanowicz, B. (2003), Global mantle tomography: Progress status in the past 10 years, *Annu. Rev. Earth Planet. Sci.*, *31*, 303–328.
- Sambridge, M. (1999a), Geophysical inversion with a neighbourhood algorithm—I: Searching a parameter space, *Geophys. J. Int.*, *138*, 479–494.
- Sambridge, M. (1999b), Geophysical inversion with a neighbourhood algorithm—II: Appraising the ensemble, *Geophys. J. Int.*, *138*, 727–746.
- Stutzmann, E., and J. P. Montagner (1993), An inverse technique for retrieving higher mode phase velocity and mantle structure, *Geophys. J. Int.*, *113*, 669–683.
- Trampert, J., and J. H. Woodhouse (1995), Global phase velocity maps of Love and Rayleigh waves between 40 and 150 seconds, *Geophys. J. Int.*, *122*, 675–690.
- Trampert, J., and J. H. Woodhouse (2001), Assessment of global phase velocity models, *Geophys. J. Int.*, *144*, 165–174.
- Van Heijst, H. J., and J. H. Woodhouse (1999), Global high-resolution phase velocity distributions of overtone and fundamental-mode surface waves determined by mode branch stripping, *Geophys. J. Int.*, *137*, 601–620.
- Wessel, P., and W. H. F. Smith (1995), New version of the generic mapping tools released, *Eos Trans. AGU*, *76*, 329.
- Yoshizawa, K., and B. L. N. Kennett (2002), Non-linear waveform inversion for surface waves with a neighbourhood algorithm—Application to multimode dispersion measurements, *Geophys. J. Int.*, *149*, 118–133.

B. L. N. Kennett, Research School of Earth Sciences, Australian National University, Mills Road, Canberra, ACT 0200, Australia.

S. Lebedev, J. Trampert, and K. Visser, Faculty of Geosciences, Utrecht University, Budapestlaan 4, NL-3584 CD Utrecht, Netherlands. (kvis@geo.uu.nl)